 CMES, vol.118, no.1, pp.139-155, 2019

Centrifuge Model Tests and Numerical Simulations of the Impact of Underwater Explosion on an Air-Backed Steel Plate

Zhijie Huang[1, 2, 3], Zuyu Chen[1, 2, 3], Xiaodan Ren[4, *], Jing Hu[3], Xuedong Zhang[3] and Lu Hai[4]

Abstract: Damage and threats to hydraulic and submarine structures by underwater explosions (UNDEXs) have raised much attention. The centrifuge model test, compared to prototype test, is a more promising way to examine the problem while reducing cost and satisfying the similitude requirements of both Mach and Froude numbers simultaneously. This study used a systematic approach employing centrifuge model tests and numerical simulations to investigate the effects of UNDEXs on an air-backed steel plate. Nineteen methodical centrifuge tests of UNDEXs were conducted. The shock wave pressure, bubble oscillation pressure, acceleration and the strain of the air-backed steel plate were recorded and compared with numerical studies using the finite element analysis (FEA) commercial software ABAQUS. By implementing empirically derived and physically measured pressures into the numerical models, the effects of the shock wave and bubble oscillation on the steel plate were investigated. Generally, the numerical results were in agreement with the experimental results. These results showed that the peak pressure of an UNDEX has a significant effect on the peak acceleration of the steel plate and that the impulse of the UNDEX pressure governs the peak strain of the steel plate.

Keywords: Centrifuge model tests, numerical simulation, underwater explosion, shock wave, bubble oscillation.

1 Introduction

Ever since the British Bomber Command destroyed the Mohne, the Eder, and the Sorpe dams located in the Ruhr Valley in Germany during World War II [Brickhill (1951)], threats by underwater explosions (UNDEXs) have been a major concern for civil and navy defense equipment and structures. In explosion engineering, reliable prediction of the dynamic response has been an important research goal [Keil (1961); Jin and Ding (2011)]. There are two parts to the impact of an UNDEX, namely, the shock wave and the bubble oscillation [Cole (1948)]. A shock wave usually hits the object instantly with

[1] MOE Key Laboratory of Soft Soils and Geoenvironmental Engineering, Zhejiang University, Hangzhou, 310058, China.

[2] Institute of Geotechnical Engineering, Zhejiang University, Hangzhou, 310058, China.

[3] China Institute of Water Resources and Hydropower Research, Beijing, 100048, China.

[4] School of Civil Engineering, Tongji University, Shanghai, 200092, China.

[*] Corresponding Author: Xiaodan Ren. Email: rxdtj@tongji.edu.cn.

high pressure. It is then followed by a series of bubble pulses induced by the expansion and contraction of the bubbles, which last for a comparatively much longer period resulting in relatively small but sustaining oscillating pressures [Cole (1948); Vernon (1986)]. Both parts of the impact are equally damaging [Snay (1957)]. The traditional model tests of UNDEX under terrestrial gravity cannot satisfy the scaling law, which requires both the Mach and the Froude numbers to be identical between the physical prototype and the scale-down model [Snay (1962)]. Navy defense sectors have made tremendous efforts to perform the destructive tests on warships since World War II [Vernon (1986); Wolf and Usnr (1970); Reid (1996)]. For example, the U.S. Navy conducted shock trials for three prototype ships in 1994 [Shin and Schneider (2003)], 2001 [Shin and Schneider (2003)], and 2008 [Schroeder (2009)]. Tens of millions of US dollars were spent in these tests [Shin and Schneider (2003)], which is an indication of low cost-effectiveness.

In past decades, studies were carried out in the centrifuge UNDEX tests. Price et al. [Price, Zuke and Infosino (1964)] investigated the scaling laws of UNDEXs for centrifugal model experiments to show that the similitude requirements of both the Mach and the Froude numbers can be satisfied. In recent years, Vanadit-Ellis et al. [Vanadit-Ellis and Davis (2010)] conducted a series of UNDEX centrifugal tests on concrete gravity dams. De et al. [De, Niemiec and Zimmie (2017)] investigated the dynamic response of a tunnel buried below submerged ground in a centrifuge. However, research on centrifugal UNDEX numerical modeling has not been extensively reported.

In this study, 19 centrifuge model tests of UNDEXs were carried out systematically [Hu, Chen, Zhang et al. (2017); Song, Chen, Long et al. (2017); Long, Zhou, Liang et al. (2017)]. They comply with a generalized scaling law based on eight πs in terms of Mach and Froude numbers. Test data have demonstrated the applicability of centrifuge tests in UNDEX [Hu, Chen, Zhang et al. (2017); Song, Chen, Long et al. (2017)]. Further, an open access database[1] has been developed to freely share all the experimental data [Long, Zhou, Liang et al. (2017)].

In view of the high expense of physical tests and limitation of test results, which cannot be extended to other situations not covered in the physical tests, numerical simulations based on the physical test procedures were carried out. After the accuracy of the numerical simulation model results were verified against the available experimental results, the model could be applied to other broader scenarios.

Information from the 19 tests contained in this database can be used for development of a numerical model to further explore other mechanical behavior of equipment and structures that are subjected to UNDEXs. In this study, the numerical model for Undex-3 by ABAQUS has been developed and the results have been verified with the experimental results [Song, Chen, Long et al. (2017); Long, Zhou, Liang et al. (2017)].

[1] http://www.geoeng.iwhr.com/geoeng/download.htm

2 Experimental model and results

2.1 Experimental model

Fig. 1 shows a schematic diagram of the UNDEX experimental setup [Song, Chen, Long et al. (2017)]. The aluminum alloy container with an internal size of 1280 mm×720 mm×950 mm is fixed onto the centrifuge basket. The steel plate with the dimensions of 600 mm×700 mm×50 mm is anchored by the cement sand. The pressure sensor is fixed on a steel stick. The depth of water in the container is 600 mm. *R* is the practical distance of the explosive to the pressure sensor. *L* is the standoff distance of the explosive to the steel plate, and *D* is the depth of the explosive.

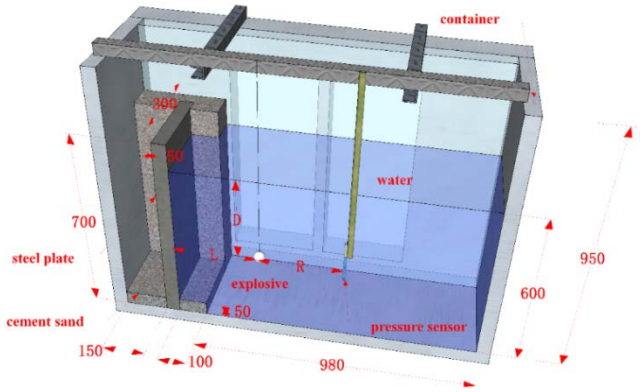

Figure 1: Schematic diagram of the 1/2 UNDEX experimental setup with dimensions in mm

Tests were conducted with different explosive mass *W*, centrifuge acceleration *G*, explosive depth *D*, and standoff distance *L*. The dynamic responses of the downstream surface of the steel plate were recorded with strain gauges and accelerometers as shown in Fig. 2.

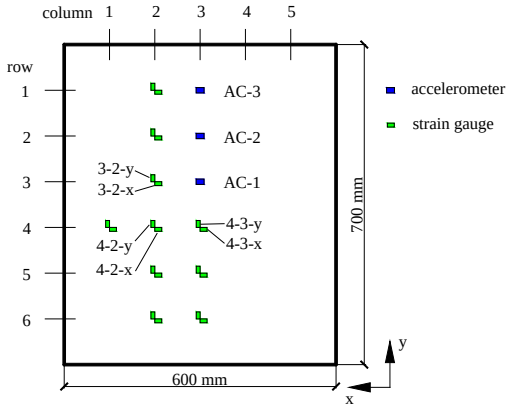

Figure 2: Layout of the strain gauges and the accelerometers

2.2 UNDEX test results

Due to the complexity of UNDEXs, to specify the UNDEX pressure by an analytical method was not straightforward. Empirical predictions for the explosion pressure were used to evaluate the objectivity of the test results. Cole [Cole (1948)] developed empirical formulas which can predict the shock wave pressure of UNDEXs. Zamyshlyaev et al. [Zamyshlyaev and Yakovlev (1973)] extended Cole's formulas to predict the bubble oscillation pressure. Thus, the pressure time-history was derived and compared with the experimental results in this research using the Cole and Zamyshlyaev and Yakovlev's (denoted by the abbreviation form of "C&Z") theory [Cole (1948); Zamyshlyaev and Yakovlev (1973)].

2.2.1 UNDEX loads from C&Z theory

From the C&Z theory, the shock wave pressure is [Cole (1948)]

$$P(t) = P_{\mathrm{m}} e^{-t/\theta} \tag{1}$$

$$P_{\mathrm{m}} = K_1 \left(\frac{W^{1/3}}{R} \right)^{\alpha_1} \tag{2}$$

$$\theta = K_2 W^{1/3} \left(\frac{W^{1/3}}{R} \right)^{\alpha_2} \tag{3}$$

where $P(t)$ is the time history of the shock wave pressure; P_{m} is the shock wave peak pressure; θ is the time delay constant; t is time; W is the explosion mass; R is the practical distance from the explosive to the pressure sensor; and K_1, K_2, α_1, and α_2 are the parameters which could be determined experimentally. The conditions for various test cases are listed in Tab. 1, in which G, D, and L are the centrifugal acceleration, explosion depth, and the distance from the explosive to the steel plate, respectively.

From the Group I and II test cases, the values for the coefficients in Eqs. (2) and (3) were obtained as shown in Fig. 3. Specifically, the values of K_1, K_2, α_1, and α_2 were 73.76, 42.84, 1.143, and -0.738, respectively.

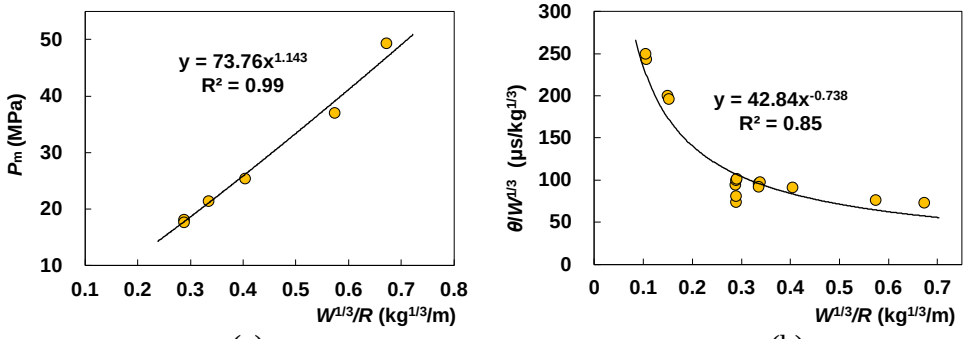

(a) (b)

Figure 3: Relationships of (a) shock wave peak pressure and (b) time delay constant versus scaled distance

Table 1: Test cases

Group	Undex-	W (g)	G (g)	R (mm)	D (m)	P_m (MPa)	θ (μs)	L (mm)
	3	1.025	40	350	0.30	17.62	8.175	300
	4	1.023	40	350	0.30	18.17	7.437	300
I	6	1.015	40	300	0.30	21.48	9.621	200
	9	1.024	40	250	0.30	25.45	9.206	250
	10	1.010	40	175	0.30	36.99	7.684	150
	11	1.025	40	150	0.30	49.32	7.344	50
	1	1.020	20	350	0.30	19.44	9.514	300
	2	1.021	30	350	0.30	18.31	10.077	300
	5	1.038	50	350	0.30	19.34	10.233	300
II	7	1.040	40	300	0.20	21.29	9.900	200
	8	1.016	20	300	0.20	20.19	9.229	200
	13	0.050	30	353.6	0.25	3.07	9.192	300
	15	0.050	20	350	0.30	3.47	8.953	300
	12	0.150	20	357.9	0.375	5.83	10.639	300
	17	0.150	40	350	0.30	4.99	10.429	300

Note: test cases of Undex-14, Undex-16, Undex-18, and Undex-19 are not listed.

The time history of the bubble oscillation pressure can be defined for 2, 4, 6-trinitrotoluene (TNT) as follows [Zamyshlyaev and Yakovlev (1973); Zong, Zhao and Zou (2014)]:

$$P(t) = P_{m1} e^{-(t-T)^2/\theta_1^2}, T - t_2 \le t < T + t_2 \tag{4}$$

$$P_{m1} = \frac{\left(39\times10^6 + 24P_0\right)R_0}{\sqrt{R^2 + D^2 - 2RD\sin\phi}} \tag{5}$$

$$\theta_1 = 20.7\frac{R_0}{P_0^{0.41}} \tag{6}$$

$$T = K_T \frac{W^{1/3}}{\left(D + D_0\right)^{5/6}} \tag{7}$$

$$t_2 = 3920\frac{R_0}{P_0^{0.71}} \tag{8}$$

where $P(t)$ is the time history of the bubble oscillation pressure; P_{m1} is the peak pressure; θ_1 is the time delay constant of the bubble oscillation pressure; T is the first period of the bubble oscillation; K_T is the coefficient with the value of 2.079 [Hu, Chen, Zhang et al. (2017)]; R_0 is the radius of the equivalent TNT explosive, which equals to $0.053W^{1/3}$

when the density of TNT was 1600 kg/m^3; D_0 is the equivalent water height of atmosphere pressure, which equaled to 10.34 m; and φ=0 is the angle between the horizontal plane and the line from the explosive to the pressure sensor.

In this study, the cyclotrimethylenetrinitramine (RDX) explosive was used instead of TNT and the conversion coefficient from RDX to TNT is 1.58 [Hu, Chen, Zhang et al. (2017)]. It should be noted that the bubble oscillation refers to the first bubble oscillation.

2.2.2 Measured loads

According to Eqs. (1)-(8), in a free field of UNDEXs, the pressure was identical for locations with similar standoff distance. Therefore, the UNDEX loads imposed on the water-plate interface with L=300 mm were equivalent to the loads measured by the pressure sensor at R=300 mm. Since the pressure sensor was located 350 mm away from the explosive, to commensurate the condition in the physical tests, the measured UNDEX pressure P was adjusted by the following formula:

$$P = P_{0.35} + \Delta P \tag{9}$$

where $P_{0.35}$ is the measured pressure at R=350 mm; and ΔP is the pressure increment when the distance shifts from 350 mm to 300 mm according to Eqs. (1)-(8).

Fig. 4 shows the time histories of the measured pressure with the amendment in Eq. (9) and the predicted pressure by the C&Z theory. The time histories of the measured and predicted pressures coincide with each other except when there were reflected waves. The measured peak pressure (denoted by Measured) and the predicted peak pressure by the C&Z theory of the shock wave were 21.60 MPa and 21.20 MPa, respectively. The corresponding peak pressures of the bubble oscillation were 0.78 MPa and 0.61 MPa, respectively.

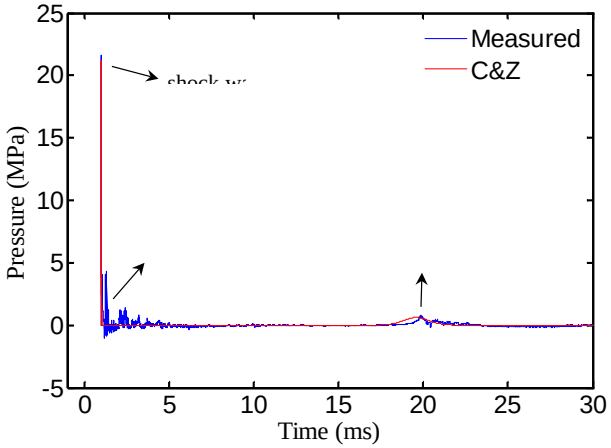

Figure 4: Time histories of UNDEX's loads of Undex-3

2.2.3 Assessment for reliability of the test results

Due to the sophisticated experimental setup and the measuring instruments, Undex-3 and Undex-4 with identical explosion parameters were carried out to exclude the potential artefacts in the centrifuge model tests and to demonstrate the repeatability of the tests as shown in Tab. 1. The results are shown in Fig. 5. Clearly, despite the high uncertainties in the nature of the tests, no significant differences were found in the results of the two tests.

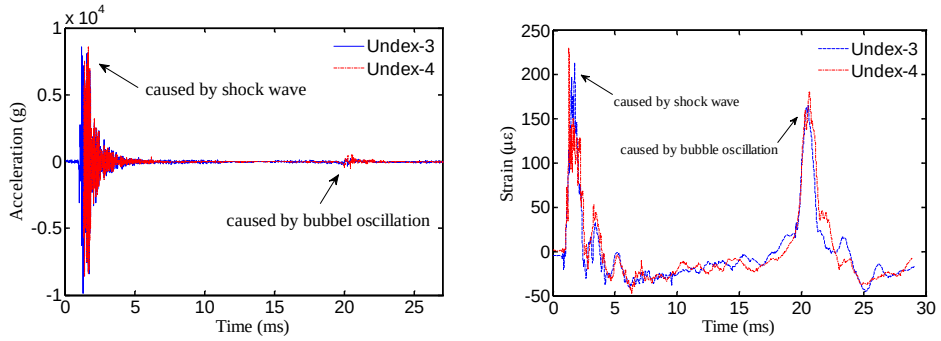

Figure 5: Results for Undex-3 and Undex-4 tests: (a) acceleration of AC-2; (b) strain of 4-3-y

From Fig. 5, it can be seen that the peak strain induced by the shock wave was approximately equal to that induced by the bubble oscillation. The ratio of the two peak strains was in the range from 0.9 to 1.6. On the other hand, the peak acceleration induced by the shock wave was much larger than that induced by the bubble oscillation. And the ratio of the two peak accelerations was in the range from 30 to 40, in spite of the peak pressure induced by the shock wave being much larger than that induced by the bubble oscillation whose ratio was about 28, as shown in Fig. 4.

The peak strains of Undex-3 are listed in Tab. 2. The results show that the average relative difference of peak strains caused by the shock wave and the bubble oscillation was 16.11%.

Table 2: Peak strains of steel plate of Undex-3

	S_s	S_b	D_r
strain 3-2-x/(10^{-6})	117.52	127.44	7.78%
strain 3-2-y/(10^{-6})	177.44	155.14	12.57%
strain 4-2-x/(10^{-6})	138.78	145.36	4.53%
strain 4-2-y/(10^{-6})	217.35	188.33	13.35%
strain 4-3-x/(10^{-6})	229.33	147.57	35.65%
strain 4-3-y/(10^{-6})	213.54	164.92	22.77%

Note: $D_r=|(S_s-S_b)/\max(S_s, S_b)|$, where S_s is the peak strain induced by the shock wave; S_b is the peak strain induced by the bubble oscillation; and D_r is the relative difference of the two peak strains.

3 Numerical model and results

3.1 Theoretical background

The simulation in this paper was based on the software package ABAQUS/Explicit, in which the "scattered wave" formula was used to study the dynamic responses of the steel plate [Zong, Zhao and Li (2013)]. The acoustic-structure coupling method was used, where water was employed as the acoustic medium. When the shock wave hit the plate, a scattered wave field was formed. The resultant velocity of the fluid particle in the fluid-structure interface region was equal to the velocity of structure. Fig. 6 shows the theoretical fluid-structure model based on experimental setup, in which the boundaries of this model are defined as follows: fluid-structure interface is S_{fs}, the non-reflecting boundary is S_{fi}, the specific pressure surface (free surface) is S_{fp}, and the reflecting boundary is S_{fr}. It should be noted that the final numerical model and conditions for simulation may not be totally the same with the model based on experimental setup as shown in Fig. 6 due to the complexity of the experimental model.

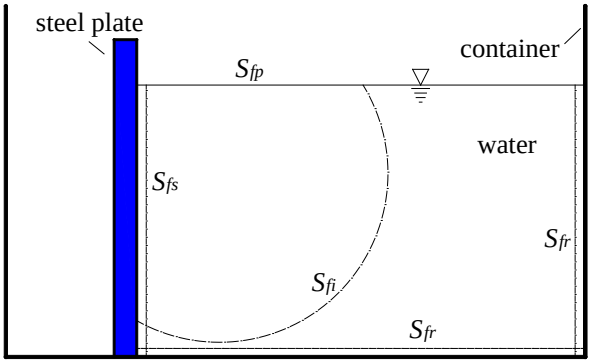

Figure 6: Fluid domain and boundaries

The dynamic equation of the fluid in the variation form is given by Eq. (10).

$$\int_{V_f}\left(\delta p\frac{\ddot{p}}{K_f}+\frac{1}{p_f}\delta p\cdot\nabla p\right)\mathrm{d}V-\int_{S_{ft}}\delta pT\mathrm{d}S_0+\int_{S_{fr}}\delta p\left(\frac{1}{c_1}\dot{p}+\frac{1}{k_1}\ddot{p}\right)\mathrm{d}S$$
$$+\int_{S_{ft}}\delta p\left(\frac{1}{c_1}\dot{p}+\frac{1}{a_1}p\right)\mathrm{d}S-\int_{S_{fs}}\delta p\boldsymbol{n}\cdot\dot{\boldsymbol{v}}_m\mathrm{d}S+\int_{S_{frs}}\left[\delta p\left(\frac{1}{c_1}\dot{p}+\frac{1}{k_1}\ddot{p}\right)-\boldsymbol{n}\cdot\dot{\boldsymbol{v}}_m\right]\mathrm{d}S=0 \tag{10}$$

where p is the pressure on the interface; $\dot{p}$ and $\ddot{p}$ are the respective first and second derivatives of pressure with respect to time; K_f is the bulk modulus of water with the value of 2140.4 MPa; c_1, k_1, α_1 are the impendence parameters determined by the boundaries; $\boldsymbol{n}$ is the normal vector pointing out from the structure; $\boldsymbol{v}_{\mathrm{m}}$ and $\dot{\boldsymbol{v}}_m$ are the respective velocity and acceleration of structure nodes; and T is the "tension" on the boundaries, which are given as follows: (1) S_{fp}: δp=0; (2) S_{ft}: $T_{ft}(\boldsymbol{x})\equiv T_0$; (3) S_{fs}: $T_{fs}(\boldsymbol{x})\equiv$

$\boldsymbol{n}\cdot\dot{\boldsymbol{v}}_m$; (4) S_{fr}: $T_{fr}(\boldsymbol{x})\equiv-\left(\dot{p}/c_1+\ddot{p}/k_1\right)$; (5) S_{fi}: $T_{fi}(\boldsymbol{x})\equiv-\left(\dot{p}/c_1+p/\alpha_1\right)$; (6) S_{frsi}: $T_{frs}(\boldsymbol{x})\equiv\boldsymbol{n}\cdot\dot{\boldsymbol{v}}_m-\left(\dot{p}/c_1+\ddot{p}/k_1\right)$.

The dynamic equation of the structure according to the virtual work theory is represented by Eq. (11).

$$\int_V \delta\boldsymbol{\varepsilon}:\boldsymbol{\sigma}\mathrm{d}V+\int_V \alpha_c\rho\delta\boldsymbol{u}_m\cdot\boldsymbol{v}_m\mathrm{d}V+\int_V \rho\delta\boldsymbol{u}_m\cdot\dot{\boldsymbol{v}}_m\mathrm{d}V+\int_{S_{fs}} p\delta\boldsymbol{u}_m\cdot\boldsymbol{n}\mathrm{d}S-\int_{S_t}\delta\boldsymbol{u}_m\cdot\boldsymbol{t}\mathrm{d}S=0 \quad (11)$$

where $\boldsymbol{\sigma}$ is the stress on structure nodes; $\delta\boldsymbol{\varepsilon}$ and $\delta\boldsymbol{u}_\mathrm{m}$ are the respective virtual strain increment and displacement increment of the structure; and $\boldsymbol{t}$ is the external force exerted on the structure's surface.

To discretize the equations, the interpolating functions are employed:

$$p=H^Q p^Q;\ \boldsymbol{u}_m=\boldsymbol{N}^M u^M;\ \delta p=H^R\delta p^R;\ \delta\boldsymbol{u}_m=\boldsymbol{N}^N\delta u^N \quad (12)$$

where the superscripts Q and R are the degrees of freedom for pressure in fluid, while M and N are the degrees of freedom for structure.

Transforming Eqs. (10) and (11) into matrix form yields Eqs. (13) and (14).

$$\left(\boldsymbol{M}_f+\boldsymbol{M}_{fr}\right)\ddot{\boldsymbol{p}}+\boldsymbol{C}_{fr}\dot{\boldsymbol{p}}+\left(\boldsymbol{K}_f+\boldsymbol{K}_{fi}\right)\boldsymbol{p}=+\boldsymbol{S}_{fs}\ddot{\boldsymbol{u}}^M+R_f \quad (13)$$

$$\boldsymbol{M}\ddot{u}+\boldsymbol{C}_{(m)}\dot{\boldsymbol{u}}+\boldsymbol{I}=-\boldsymbol{S}_{fs}^{\mathrm{T}}\boldsymbol{p}+R \quad (14)$$

where the matrixes are:

$$\begin{cases} M_f^{RQ}=\int_{V_f}\frac{1}{K_f}H^RH^Q\mathrm{d}V, M_{fr}^{RQ}=\int_{S_{fr}\cup S_{frs}}\frac{1}{k_1}H^RH^Q\mathrm{d}S, K_f^{RQ}=\int_{V_f}\frac{1}{\rho_f}\nabla H^R\cdot\nabla H^Q\mathrm{d}V \\ C_{fr}^{RQ}=\int_{S_{fr}\cup S_{frs}}\frac{1}{c_1}H^RH^Q\mathrm{d}S+\int_{S_{fi}}\frac{1}{c_1}H^RH^Q\mathrm{d}S, K_{fi}^{RQ}=\int_{S_{fi}}\frac{1}{a_1}H^RH^Q\mathrm{d}S \\ S_{fs}^{RM}=\int_{S_{fs}\cup S_{frs}}H^R\boldsymbol{n}\cdot\boldsymbol{N}^M\mathrm{d}S, R_f^R=\int_{S_{ft}}H^RT_0\mathrm{d}S, M^{NM}=\int_V\rho\boldsymbol{N}^N\cdot\boldsymbol{N}^M\mathrm{d}V \\ C_{(m)}=\int_V\alpha_c\rho\boldsymbol{N}^N\cdot\boldsymbol{N}^M\mathrm{d}V, I^N=\int_V\boldsymbol{\beta}^N:\boldsymbol{\sigma}\mathrm{d}V, R^N=\int_{S_t}\boldsymbol{N}^N\cdot\boldsymbol{t}\mathrm{d}S \end{cases} \quad (15)$$

In the above equations, $\boldsymbol{\beta}^N$ is the strain transform tensor; $\boldsymbol{\beta}^N$:$\boldsymbol{\sigma}$ is the second contraction of tensor; and $S_{fs}^{RM}\ddot{u}^M$, $\left[S_{fs}^{QN}\right]^T p^Q$ are the respective force applied to fluid and structure.

The fluid pressure and structure displacement were obtained by solving Eqs. (13) and (14) with the Newmark method or Wilson-θ method. The numerical simulation for UNDEXs is based on the central difference formula, which was embedded in ABAQUS/Explicit.

3.2 Numerical model

To further explore the impact of the explosion pressure on a target structure, the spherical incident waves of the C&Z pressure and the measured pressure (Fig. 4) were applied to the water-plate coupling interface in the numerical model, which was created using

ABAQUS. Fig. 7 shows the numerical model used to reproduce the procedure in the experiments. The C3D8R eight-node solid elements were used for the steel plate and the cement sand with the element dimension of 12.5 mm, and the AC3D8R acoustic elements were used for water with the element dimension of 5 mm. The whole model contains 377,782 nodes and 353,572 elements.

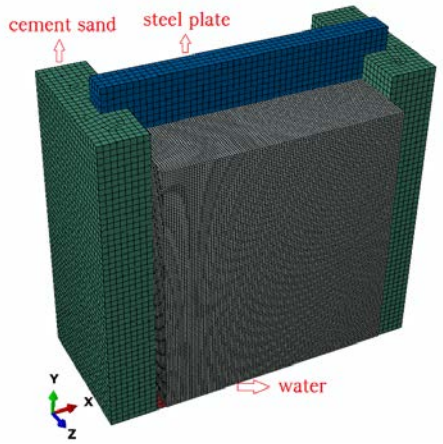

Figure 7: Numerical model created in ABAQUS

3.2.1 Material parameters

The relevant material parameters used in the numerical model are shown in Tab. 3.

Table 3: Material parameters

	Density (kg/m^3)	Young's/Bulk modulus (GPa)	Poisson's ratio
Steel plate	7850	206	0.3
Cement sand	2400	29.5	0.3
Water	1000	2.140	-

3.2.2 Boundary and loading conditions

In the numerical model, the boundaries of the cement sand were fixed. The surface-to-surface contact was applied between the cement sand and the steel plate using the penalty function method for mechanical constraint formulation and finite sliding for the sliding formulation. The friction coefficient of 0.8 was selected in the penalty friction formulation for tangential behavior and "hard contact" was used for normal behavior. The "TIE" constraint was applied to the interface of the water and the steel plate, which simulated the fluid-structure interaction with the surface of structure as the master surface and the surface of water as the slave surface. In this way, the nodes of both the water and the structure in the interface deform concurrently. The initial pressure of the free surface of water was defined as zero. To reduce the computational intensity, the simplified model with shorter length of water field and without container was created. Generally, the shock wave also impacted on the bottom and the other three side walls of the container. Then there were reflected waves and second reflected waves impacting on the steel plate again

in the same way as shock wave did except the direction. Because the wave propagation from the explosive to the steel plate was initially specified when using "scattered wave" formula in ABAQUS, the effects of wave reflection was so complex and may not be completely and correctly reflected in the simplified model by just setting reflecting boundaries, especially in the case of lack of relevant parameters. Therefore, the way that measured reflected waves served as incident waves, just like shock wave, may be a compensation for the reflected boundary, though it may not be accurate enough. The non-reflecting boundary condition was finally used for the water boundary surfaces since all the UNDEX loads, including the reflected waves, were inputted into the numerical model as the incident wave. The default damping setting in ABAQUS was used since there were no relevant data from the physical tests.

3.3 Results and discussion

In order to investigate whether the steel plate had the plastic strains or not, the ideal elastic-plastic model with the yield stress of 235 MPa was compared to the elastic model for the steel plate with the parameters shown in Tab. 3. Fig. 8 shows the simulated strain time histories of 3-2-x when using elastic and elastic-plastic model for the steel plate, respectively. It can be known that the simulated strains for these two models are nearly the same, which means that there are no plastic strains occurring in the steel plate. It can also be validated by the experimental results because the steel plate with the thickness of 5 cm was strong enough to defense the impact loading induced by UNDEX with 1 g explosive. Therefore, the elastic model for the steel plate with the parameters shown in Tab. 3 was just used in the paper.

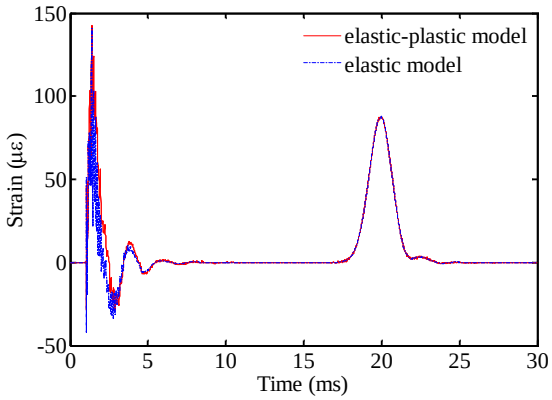

Figure 8: Numerical results of strain time histories of 3-2-x with the elastic and elastic-plastic model for the steel plate

3.3.1 Dynamic responses induced by shock wave

Fig. 9 shows the acceleration time histories of AC-2 induced by the shock wave. Fig. 9(a) shows the acceleration time history measured in the Undex-3 test. Figs. 9(b) and 9(c) show the numerically simulated acceleration time histories with the measured pressure

time history and the C&Z pressure time history. It can be seen that with regard to the peak accelerations, both the numerical results are close to the experimental result.

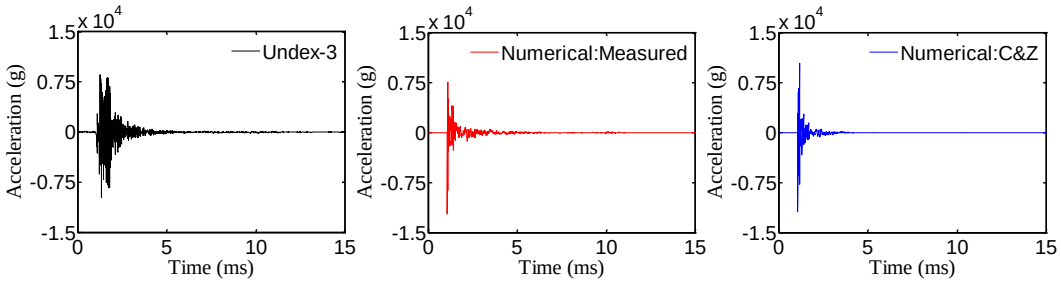

(a) (b) (c)

Figure 9: Acceleration time histories of AC-2 induced by shock wave: (a) experimental result; (b) numerical result with measured pressure; (c) numerical result with C&Z pressure

Peak accelerations are shown in Tab. 4. It can be seen that the maximum difference between the numerical and experimental peak accelerations is 23.79%, while the average difference is 21.27%.

Table 4: Peak accelerations of AC-2 induced by the shock wave

	A_t	$A_{C\&Z}$	D_{ar}	A_M	D_{ar}
positive peak acceleration/(g)	8591.80	10447.66	21.60%	7664.38	10.79%
negative peak acceleration/(g)	-9841.93	-11903.54	20.95%	-12183.79	23.79%

Note: $D_{ar}=|(A_{C\&Z}-A_t)/A_t|$ or $|D_{ar}=(A_M-A_t)/A_t|$, where A_t, $A_{C\&Z}$, and A_M are the respective peak accelerations from the test, the numerical results with the C&Z pressure and the measured pressure; and D_{ar} is the relative percentage difference of the peak accelerations.

Fig. 10 shows the numerical results of the strain time histories induced by the shock wave. Generally, both strain time histories with the C&Z pressure and the measured pressure are similar to that of the experimental result. On the other hand, the numerical results attenuated quicker than the experimental result, especially in the *y*-direction, as shown in Figs. 10(b) and 10(d). This may be attributed to the assumed boundary condition in the numerical model. The steel plate was embedded in the cement sand supports. So, the real boundary condition was complicated, which may not be effectively reflected in the numerical model by using the fixed or simply supported boundary conditions.

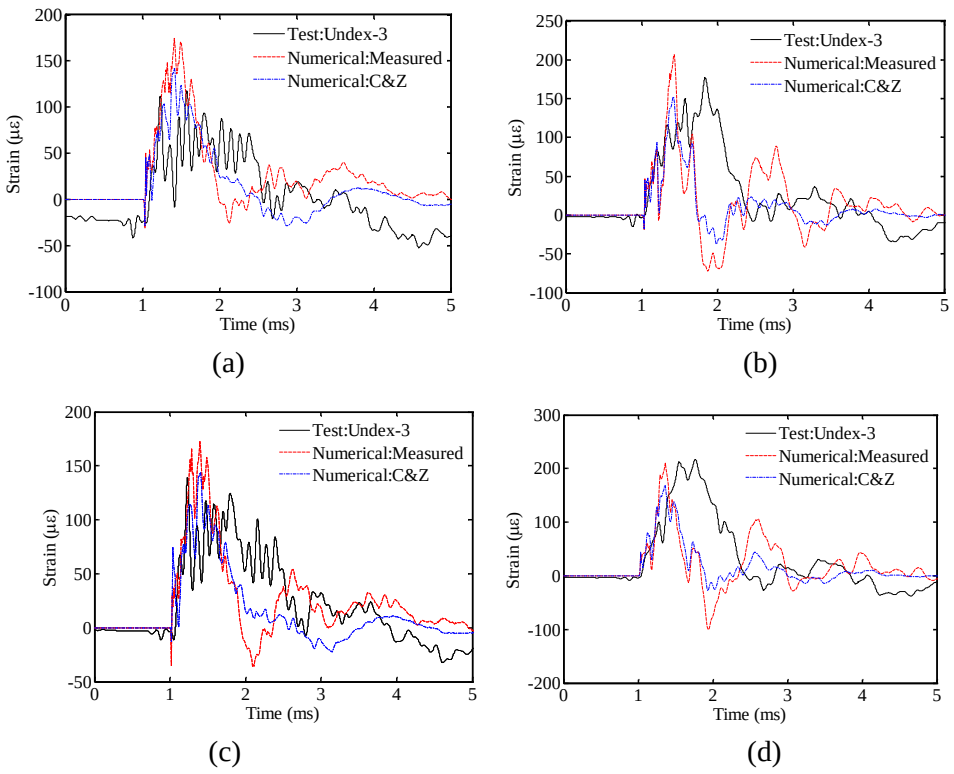

Figure 10: Strain time histories induced by shock wave at (a) 3-2-x; (b) 3-2-y; (c) 4-2-x; (d) 4-2-y

Table 5: Peak strains of the steel plate caused by shock wave

	S_t	$S_{C\&Z}$	D_{sr}	S_M	D_{sr}
strain 3-2-x/(10^{-6})	117.52	142.31	21.09%	174.47	48.46%
strain 3-2-y/(10^{-6})	177.44	152.07	14.30%	206.68	16.48%
strain 4-2-x/(10^{-6})	138.78	143.80	3.62%	172.50	24.30%
strain 4-2-y/(10^{-6})	217.35	169.06	22.22%	210.31	3.24%

Note: $D_{sr}=|(S_{C\&Z}-S_t)/S_t|$ or $|D_{sr}=(S_M-S_t)/S_t|$, where S_t, $S_{C\&Z}$, and S_M are the peak strains of the experimental result, the numerical results by the C&Z empirical pressure, and the measured pressure, respectively; D_{sr} is the relative percentage difference of the peak strains.

Tab. 5 shows a comparison of the peak strains of the experimental and numerical results. It can be seen that the relative percentage difference D_{sr} of the peak strains of the C&Z pressure were substantially less than those of the measured pressure except for 4-2-y. The maximum percentage differences of the peak strains by the C&Z pressure and the measured

pressure were 22.22% in the *y*-direction and 48.46% in the *x*-direction. Further, the corresponding average percentage differences of the peak strains were 15.31% and 23.12%.

3.3.2 Dynamic responses induced by bubble oscillation

Fig. 11 shows the acceleration time histories of AC-2 induced by the bubble oscillation. It can be seen that both the trends of numerical acceleration time histories are similar to that of the experimental time history. On the other hand, as compared to the peak acceleration of the experimental result, the relative percentage difference of the numerical results with the C&Z pressure is higher than that with the measured pressure.

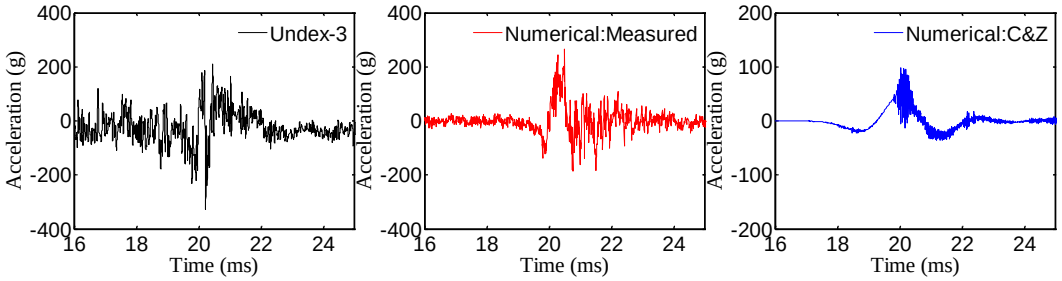

Figure 11: Acceleration time histories of AC-2 induced by shock wave: (a) experimental result; (b) numerical result with measured pressure; (c) numerical result with C&Z pressure

Fig. 12 shows the numerical results of strain time histories induced by the bubble oscillation pressure. It can be seen that they are similar to that of the experimental result. However, as shown in Figs. 12(b) and 12(d), both the numerical peak strains are smaller than the experimental peak strain, especially in the *y*-direction. This may result from the improper time history of bubble oscillation due to the limitation of Zamyshlyaev and Yakovlev's formulas and the measurement error. An examination of the numerical results showed that the bubble oscillation pressures in the numerical models with the C&Z pressures and the measured pressures were smaller than the practical explosion pressure impinged on the steel plate. On the other hand, further inefficiency may also arise from the unrealistic modelling of the fluid-structure interaction between the steel plate and the water due to uncertainties in the specification of the interaction parameters. Hence, the accuracy of the pressure history input into the numerical model had a great influence on the numerical results, which deserves further investigation. It is worth noting that as shown in Fig. 4, the measured pressure of the bubble oscillation abruptly decreased to negative at approximately 20.5 ms. In the numerical strain time history, this leads to a sudden fall with the measured pressure especially in the vertical direction, as shown in Fig. 12.

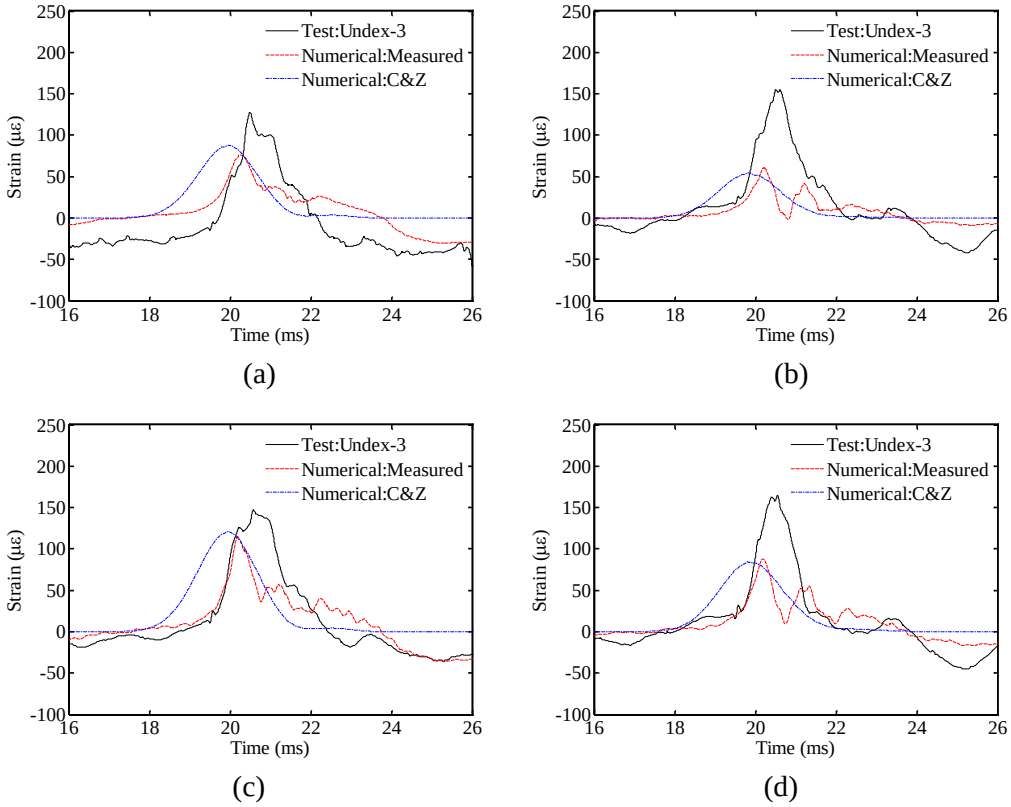

Figure 12: Strain time histories caused by bubble oscillation: (a) 3-2-x; (b) 3-2-y; (c) 4-3-x; (d) 4-3-y

As mentioned in Section 2.2.3, the experimental results showed that the peak strains induced by the shock wave were approximately equivalent to those induced by the bubble oscillation. Similarly, the pressure impulse of the shock wave was approximately equivalent to that of the bubble oscillation. On the other hand, the peak accelerations induced by the shock wave were much higher than those induced by the bubble oscillation. The trends for the peak pressures were similar. Thus, it can be concluded that the peak pressure of UNDEX had a significant effect on the peak acceleration of the steel plate, whereas the impulse of the UNDEX loads governed the peak strain of the steel plate.

4 Conclusions

In this study, a systematic approach was carried out using centrifuge model tests and numerical simulations to investigate the effects of the underwater explosions on an air-backed steel plate. The pressure of UNDEX loads, the acceleration, and the strain of the downstream surface of the steel plate were measured experimentally and simulated numerically. From the numerical simulations, the impact effects of the shock wave and the bubble oscillation pressure on the dynamic response of the steel plate were

investigated. Based on the experimental and numerical results, the following conclusions were drawn.

(1) The experimental results showed that the peak strains induced by the shock wave were approximately equal to those induced by the bubble oscillation with the range of ratios from 0.9 to 1.6, although the peak pressure induced by the shock wave was much larger than that induced by the bubble oscillation with the ratio of 28. On the other hand, the peak accelerations induced by the shock wave were much larger than those induced by bubble oscillation, and the ratio of the two peak accelerations is in the range from 30 to 40.

(2) Generally, the numerical results were in agreement with the respective experimental results. However, the average differences of the peak strains and peak accelerations caused by the bubble oscillation compared to the experimental results were slightly larger than those caused by shock wave.

(3) The numerical and experimental results showed that the peak pressure of UNDEX had a significant effect on the peak acceleration of the steel plate, while the impulse of the UNDEX loads governed the peak strain of the steel plate.

Acknowledgments: The authors would like to thank Prof. Guowei Ma, Prof. Fang Wang, and Prof. Hongyuan Zhou for critically reading and revising the manuscript as well as for helpful discussions. This study has been financially supported by the State Key Program of National Natural Science Foundation of China (Grant No. 51339006).

References

Brickhill, P. (1951): *The Dam Busters*. Pan Books, London.

Cole, R. H. (1948): *Underwater Explosions*. Princeton University Press, New Jersey, USA.

De, A.; Niemiec, A.; Zimmie, T. F. (2017): Physical and numerical modeling to study effects of an underwater explosion on a buried tunnel. *Journal of Geotechnical and Geoenvironmental Engineering*, vol. 143, no. 5, 04017002.

Hu, J.; Chen, Z. Y.; Zhang, X. D.; Wei, Y. Q; Liang, X. Q. et al. (2017): Underwater explosion in centrifuge part I: validation and calibration of scaling law. *Science China Technological Sciences*, vol. 60, no. 11, pp. 1638-1657.

Jin, Q. K.; Ding, G. Y. (2011): A finite element analysis of ship sections subjected to underwater explosion. *International Journal of Impact Engineering*, vol. 38, no. 7, pp. 558-566.

Keil, A. H. (1961): *The Response of Ships to Underwater Explosions*. David Taylor Model Basin Washington DC, New York, USA.

Long, Y.; Zhou, H. Y.; Liang, X. Q.; Song, G.; Chen, Z. Y. et al. (2017): Underwater explosion in centrifuge part II: dynamic responses of defensive steel plate. *Science China Technological Sciences*, vol. 60, no. 12, pp. 1941-1957.

Price, R. S.; Zuke, W. G.; Infosino, C. (1964): *A Study of Underwater Explosions in a High Gravity Tank*. Naval Ordnance Lab White Oak MD, Maryland, USA.

Reid, W. D. (1996): *The Response of Surface Ships to Underwater Explosions*. Defense

Science and Technology Organization, Canberra, Australia.

Schroeder, D. (2009): Shock waves rock USS MESA VERDE. *Currents*, pp. 20-27.

Shin, Y. S.; Schneider, N. A. (2003): Ship shock trial simulation of USS Winston S. Churchill (DDG 81): modeling and simulation strategy and surrounding fluid volume effects. *74th Shock and Vibration Symposium*, pp. 26-31.

Snay, H. G. (1957): Hydrodynamics of underwater explosions. *Symposium on Naval Hydrodynamics*, pp. 515-325.

Snay, H. G. (1962): *The Scaling of Underwater Explosion Phenomena*. Naval Ordnance Lab White Oak MD, Maryland, USA.

Song, G.; Chen, Z. Y.; Long, Y.; Zhong, M. S.; Wu, J. Y. (2017): Experimental and numerical investigation of the centrifugal model for underwater explosion shock wave and bubble pulsation. *Ocean Engineering*, vol. 142, pp. 523-531.

Vanadit-Ellis, W.; Davis, L. K. (2010): Physical modeling of concrete gravity dam vulnerability to explosions. *Waterside Security Conference*, pp. 1-11.

Vernon, T. A. (1986): *Whipping Response of Ship Hulls from Underwater Explosion Bubble Loading*. Defense Research Establishment Atlantic, Dartmouth (Nova Scotia), Canada.

Wolf, N. M.; Usnr, L. M. (1970): *Underwater Blast Injury-A Review of the Literature*. Naval Submarine Medical Center, Virginia, USA.

Zamyshlyaev, B. V.; Yakovlev, Y. S. (1973): *Dynamic Loads in Underwater Explosion*. Naval Intelligence Support Center Washington DC Translation Div, Washington, USA.

Zong, Z.; Zhao, Y. J.; Li, H. T. (2013): A numerical study of whole ship structural damage resulting from close-in underwater explosion shock. *Marine Structures*, vol. 31, pp. 24-43.

Zong, Z.; Zhao, Y. J.; Zou, L. (2014): *Numerical Computation for Structural Damages of Underwater Explosion*. Science Press, Beijing (In Chinese).